Crystal Growth and Characterization of Type III Ytterbium-Doped $KGd(PO_3)_4$: A New Nonlinear Laser Host

I. Parreu, R. Solé, J. Massons, F. Díaz, and M. Aguiló*

Física i Cristal·lografia de Materials (FiCMA), Universitat Rovira i Virgili. Campus Sescelades. C/Marcel·lí i Domingo, s/n 43007, Tarragona, Spain

Received September 8, 2006. Revised Manuscript Received February 14, 2007

We determined how evolved the $P2_1$ crystallization region of ytterbium-doped $KGd(PO_3)_4$ (Yb:KGP) as a function of the ytterbium concentration in the composition region close to that previously determined as the optimum region to grow single crystals of undoped KGP. In this region, the border between the polymorphs $KYb_xGd_{1-x}(PO_3)_4$ with long-chain geometry and $KYb_xGd_{1-x}P_4O_{12}$ with cyclical geometry varied depending on the ytterbium concentration. Inclusion-free single crystals of Yb:KGP were successfully grown using the top-seeded solution growth technique under conditions similar to those of KGP. Ytterbium doping in KGP was proved to be possible and effective. The effect of the ytterbium doping on structural and optical properties of the KGP host was determined. We found that Yb:KGP decomposed irreversibly at 1130 K. The vibrational structure of both KGP and Yb:KGP was found to be similar to other metaphosphates. The spectroscopic properties of ytterbium in the KGP host were analyzed.

Introduction

Currently, a great range of wavelengths from the ultraviolet to the infrared are needed for a huge variety of applications such as high-density optical data storage, color displays, biotechnology, medicine, submarine communications, transparent atmosphere applications, etc. These wavelengths can be managed from frequency conversion of a given laser emission by nonlinear optical processes such as frequency doubling. Attractive crystals for frequency conversion are bifunctional laser and optical materials, in which the laser effect and the nonlinear optical process occur simultaneously inside the same host. A self-frequency doubling (SFD) laser has lower losses, i.e., reflections, absorption, scattering losses, and leads to a simpler and more compact laser device. This advantage can be added to the others that come using solid-state laser sources such as efficiency, low maintenance and cost, and the possibility to be diode pumped. Since the first demonstration of SFD laser action in the green region from Nd-doped $MgO:LiNbO_3$,[1] a great effort was focused on searching new nonlinear laser crystals capable of generating SFD laser radiation in the visible. Up to now, SFD in the visible has been proved in several Nd- and Yb-doped nonlinear crystals.[2,3] The 1 μm laser emission of these ions can be combined with the second harmonic generation properties of the nonlinear host to produce green laser radiation by SFD. The ytterbium ion is an interesting alternative to neodymium in the same wavelength range near 1 μm because of several important advantages.[4−7] The ytterbium ion has a longer energy-storage capability because of the longer radiative lifetime of the upper laser manifold, about three or four times longer. The simple two-manifold electronic structure of ytterbium excludes a variety of competitive processes that can depopulate the upper laser level and hence reduce the laser efficiency. The small Stokes shift between absorption and emission, i.e., quantum defect, reduces the thermal load and gives efficient operation at high powers. Finally, ytterbium is totally transparent in the green region, so the inevitable reabsorption losses of neodymium in the wavelength range of the second harmonic can be avoided. For the same reason, the nonlinear host should also be transparent at the generated wavelength range. More recently, highly efficient laser operation in some nonlinear crystals doped with ytterbium has been furthermore reported.[2,3,8−13] As a rule, a self-frequency doubling crystal must (i) accept fluorescent ion doping and (ii) be phase-matchable for its laser emission. The potentiality of these crystals relies on a strong and wide pump absorption bandwidth as well as on a relative gain cross-section.

We propose in this paper a new candidate to self-frequency doubling laser material Yb-doped $KGd(PO_3)_4$ (Yb:KGP)

* To whom correspondence should be addressed. E-mail: magdalena.aguilo@urv.net.

(1) Fan, T. Y.; Cordova-Plaza, A.; Digonnet, M. J. F.; Byer, R. L.; Shaw, H. J. *J. Opt. Soc. Am. B* **1986**, *3* (1), 140.
(2) Brenier, A. *J. Lumin.* **2000**, *91* (3−4), 121.
(3) Brenier, A.; Jaque, D.; Majchrowski, A. *Opt. Mater.* **2006**, *28* (4), 310
(4) DeLoach, L. D.; Payne, S. A.; Chase, L. L.; Smith, L. K.; Kway, W. L.; Krupke, W. F. *IEEE J. Quantum Electron.* **1993**, *29* (4), 1179.
(5) Krupke, W. F. *IEEE J. Quantum Electron.* **2000**, *6* (6), 1287.
(6) Zou, X.; Toratani, H. *Phys. Rev. B* **1995**, *52* (22), 15889.
(7) Mateos, X.; Petrov, V.; Aguiló, M.; Solé, R.; Gavaldà, Jna.; Massons, J.; Díaz, F.; Griebner, U. *IEEE J. Quantum Electron.* **2004**, *40* (8), 1056.
(8) Brenier, A. *J. Lumin.* **2000**, *92* (3), 199.
(9) Mougel, F., Dardenne, K.; Aka, G.; Kahn-Harari, A.; Vivien, D. *J. Opt. Soc. Am. B* **1999**, *16* (1), 164.
(10) Richardson, M.; Hammons, D.; Eichenholz, J.; Chai, B. H. T.; Ye, Q.; Jang, W. K.; Shah, L. *J. Korean Phys. Soc.* **2000**, *37* (5), 633.
(11) Dekker, P.; Burns, P. A.; Dawes, j. M.; Piper, J. A. *J. Opt. Soc. Am. B* **2003**, *20* (4), 706.
(12) Bausá, L. E.; Ramírez, M. O.; Montoya, E. *Phys. Status. Solidi* **2004**, *201* (2), 289.
(13) Montoya, E.; Sanz-García, J. A.; Capmany, J.; Bausá, L. E.; Diening, A.; Kellner, T.; Huber, G. *J. Appl. Phys.* **2000**, *87* (9), 4056.

10.1021/cm0621242 CCC: $37.00
Published on Web 05/01/2007

because it satisfies all of these preliminary essential conditions. The KGP host has a noncentrosymmetric structure; SFD can therefore originate from the second order nonlinear polarization. Type III KGP is monoclinic and has $P2_1$ as space group. The crystal cell parameters are:[14] $a = 7.255(4)$ Å, $b = 8.356(5)$ Å, $c = 7.934(5)$ Å, $\beta = 91.68(5)°$; $Z = 2$; $V = 480.80(5)$ Å^3. A priori, the gadolinium ion ensures high acceptance of rare-earth dopants in its structural site because of its privileged position in the middle of the lanthanides series, i.e., highly Nd-substituted KGP crystals[14] and even the stoichiometric isostructure of neodymium, $KNd(PO_3)_4$ (KNP),[15,16] have been synthesized. Because of the wide transparency window of KGP, which extends from 180 nm to 4 μm,[14] transparency is guaranteed at both the fundamental and the second harmonic range. This really low UV cutoff allows us in principle to use this host also in the UV range (either as a nonlinear crystal or as a host for cerium). The quite large band gap should increase the damage resistivity of the crystal, so high-power diode-pumping should be allowed. KGP presents also some promising properties to be a new candidate to nonlinear solid-state laser host such as an almost isotropic thermal expansion, which protects it from thermal deforming during laser operation[17] and a high chemical stability, which ensures that the useful life of the laser device would not be limited by its chemical degradation.[18] The highly microhardness of KGP,[18] around that of quartz , facilitates sample preparation and allows polishing of the laser surfaces with good optical quality. Yb:KGP has similar absorption and emission cross-sections[19] to those of other nonlinear ytterbium doped crystals in which SFD in the visible region has been proved, such as Yb:GdCOB,[9] Yb:YCOB,[10] Yb:YAB,[11] Yb:$LiNbO_3$,[12] and Yb:MgO:$LiNbO_3$.[13] Recently, room-temperature laser generation in the 1 μm range has been demonstrated[19] in this new Yb host for the first time. The lasing studies were based on a preliminary single $KYb_{0.024}Gd_{0.976}(PO_3)_4$ sample that was cut and polished as a cube accurately oriented along the N_p, N_m, and N_g principal optical axes with dimensions of 2.34, 2.68, and 2.47 mm along these axes, respectively. Although the size and the doping level of the sample limited the maximum output power achieved, on the order of 100 mW, the greater than 55% slope efficiency obtained with this first sample is rather promising for the future. We decided therefore to dedicate many efforts to optimizing the synthesis of Yb:KGP crystals with a higher ion-doping level.

As KGP inclusion-free single crystals can be successfully grown,[17] we studied how evolved the crystallization region and the growth process when introducing ytterbium in solution. The structural effect of ytterbium in the KGP structure was also studied, hence the variation of the crystal cell parameters a, b, c, β, and V as a function of the ytterbium concentration was determined. The thermal behavior of Yb:KGP was also analyzed in terms of phase transition and thermal evolution. A short study of Raman scattering was made to determine the phonon frequencies of the KGP and the Yb:KGP lattice. Because of its potential application as self-frequency doubling laser material, some optical and spectroscopic studies were also performed. We determined the optical transmission of Yb:KGP and compared it to that of the host. The optical absorption and emission of ytterbium in KGP at room temperature were also included.

Experimental Section

Crystallization Region of Yb:KGP. To determine the region in which ytterbium-doped KGP crystallizes as the $P2_1$ single phase (type III) from its self-flux, we grew small single crystals of several ytterbium concentrations from three different solution compositions. All these composition points were placed inside the previously determined KGP crystallization region[17] and were (Yb_2O_3+Gd_2O_3):K_2O:P_2O_5 = 6:34:60, 4:36:60, and 2:38:60 mol %. The phosphorus oxide percentage was kept constant at 60 mol %, because higher concentrations imply too much higher solution viscosities;[14,16,17] therefore, only the Ln_2O_3:K_2O ratio was varied among 15:85, 10:90, and 5:95. In each of these three solution compositions, ytterbium concentrations of 0.5, 1, 3, 5, 10, 15, 20, 30, and 50 at % were used. The desired ratios of the corresponding oxides were mixed to prepare roughly 20 g of solution in a conical platinum crucible of 25 cm^3. We used Yb_2O_3, Gd_2O_3, K_2CO_3, and $NH_4H_2PO_4$ as initial reagents. The crucible was kept in a vertical furnace with a Kantal AF heater whose temperature was measured by an S-type thermocouple and controlled by a Eurotherm 818 P controller/programmer connected to a thyristor. The axial gradient in the solution was about 5 K/mm, increasing the temperature from the surface to the bottom along around 20 mm. We determined the saturation temperature by observing the growth or dissolution of crystals spontaneously nucleated on the solution surface. From the saturation temperature, the solution was cooled at a rate of 0.1 K/h to about 12 K below. Crystals grown on a platinum disk rotating at 60 rpm placed at the center of the solution surface. To identify the crystalline phase of the small crystals grown, we used X-ray powder diffraction analysis.

X-ray Powder Diffraction. The X-ray powder diffraction technique was used to perform some structural characterizations of the Yb:KGP crystals as well as their simply identification. The experiments were carried out using the Cu Kα radiation in a D5000 Siemens X-ray powder diffractometer in a $\theta-\theta$ configuration with the Bragg−Brentano geometry and a scintillation counter as detector.

Small crystals grown on a platinum disk from fluxes containing ytterbium atomic percentages of 1, 3, 5, 10, 15, 20, 30, and 50 were analyzed to calculate the crystal cell parameters of ytterbium-doped KGP crystals. The composition of the growth solution was changed depending on the ytterbium concentration in order to ensure the crystallization of the $P2_1$ phase. The X-ray diffraction patterns were recorded in the 2θ range from 10 to 70° at a step size of 0.02° and a step time of 16 s. The crystal cell parameters were refined using the FULLPROF[20] program and the Rietveld[21] method

(14) Parreu, I.; Carvajal, J. J.; Solans, X.; Díaz, F.; Aguiló, M. *Chem. Mater.* **2006**, *18* (1), 221.
(15) Hong, H. Y-P. *Mater. Res. Bull.* **1975**, *10* (10), 1105.
(16) Parreu, I.; Solé, R.; Gavaldà, Jna.; Massons, J.; Díaz, F.; Aguiló, M. *Chem. Mater.* **2003**, *15* (26), 5059.
(17) Parreu, I.; Solé, R.; Gavaldà, Jna.; Massons, J.; Díaz, F.; Aguiló, M. *Chem. Mater.* **2005**, *17* (4), 822.
(18) Parreu, I.; Solé, R.; Massons, J.; Díaz, F.; Aguiló, M. *Cryst. Growth Design* **2007**, *7*, in press.
(19) Parreu, I.; Pujol, M. C.; Aguiló, M.; Díaz, F.; Mateos, X.; Petrov, V. *Opt. Express* **2007**, in press.
(20) Rodríguez-Carvajal, J. *Short Reference Guide for the Computer Program FULLPROF*; Laboratoire León Brillouin, CEA CNRS: Gif sur Yvette, France, 1998.
(21) Young, R. A. *The Rietveld Method*; International Union of Crystallography Monographs on Crystallography 5; Oxford University Press: Oxford, U.K., 1995.

Table 1. Growth Data Associated with Ytterbium-Doped KGP Single Crystals

growth experiment	solution composition Yb_2O_3:Gd_2O_3:K_2O:P_2O_5 (mol %)	Yb at % in solution	Yb at % in crystal	distribution coeff of Yb in KGP	$T_{saturation}$ (K)	cooling program[a]	seed orientation	cryst dimensions ($a \times b \times c$; mm^3)	crystal weight	crystal quality
1	0.04:3.96:36:60	1	0.5	0.5	889	12/0.1	**a***	$4.5 \times 6.1 \times 5.3$	0.77	good
2	0.02:1.98:38:60	1	0.3	0.32	823	12/0.1	**a***	$3.4 \times 4.9 \times 4.1$	0.49	good
3	0.18:5.82:34:60	3	1.5	0.49	943	12/0.1	**a***	$5.1 \times 7.7 \times 6.9$	0.91	some inclusions
4	0.18:5.82:34:60	3	1.6	0.53	939	12/0.05	**a***	$5.1 \times 7.4 \times 6.8$	0.89	good
5	0.3:5.7:34:60	5	2.6	0.51	952	12/0.1	**a***		0.87	polycrystalline
6	0.3:5.7:34:60	5	2.4	0.48	958	12/0.05	**a***	$4.7 \times 6.2 \times 6.1$	0.85	good
7	0.6:5.4:34:60	10	4.0	0.40	981	12/0.1	**a***		0.99	polycrystalline
8	0.6:5.4:34:60	10	4.2	0.42	975	12/0.05	**a***	$5.6 \times 8.3 \times 7.6$	1.00	some inclusions
9	0.6:5.4:34:60	10	4.0	0.40	971	2/0.02 10/0.05	**a***	$5.8 \times 6.8 \times 6.3$	0.88	good
10	0.6:3.4:36:60	15	7.7	0.51	895	2/0.02 10/0.05	**a***	$4.2 \times 6.5 \times 5.7$	0.76	good

[a] The decreased temperature interval/ rate of temperature decrease.

using the KGP structure solved previously by single-crystal X-ray diffraction,[14] as a starting model.

We also used X-ray powder diffraction analysis to check if the evolution of the crystal cell parameters of Yb:KGP and undoped KGP when increasing the temperature was comparable. We therefore analyzed a powdered sample of $KYb_{0.029}Gd_{0.971}(PO_3)_4$ small crystals grown from a solution composition of Yb_2O_3:Gd_2O_3:K_2O:P_2O_5 = 0.3:5.7:34:60 mol %. The above-described diffractometer was equipped with an Anton-Paar HTK10 platinum ribbon heating stage. The diffraction patterns were recorded in the same 2θ range at a step size of 0.03° and a step time of 5 s at temperatures of 298 and 773 K, with a delay time of 300 s before each pattern recording.

The thermal evolution of Yb:KGP from room temperature to 1273 K, both heating and cooling the sample, was also analyzed. The same powdered sample of $KYb_{0.029}Gd_{0.971}(PO_3)_4$ was used. The diffractometer was also equipped with a Braun position-sensitive detector (PSD). To compare with undoped KGP, we used the same thermal program. The sample was heated at 10 K/s from 298 to 673 K and from this point to the maximum (1273 K) at 0.17 K/s; it was then cooled using the same conditions. Diffraction patterns were registered every 50 K in the slowest heating and cooling ranges (673−1273 K) at a 2θ of 10−70° using a measuring time per degree of 10 s.

Differential Thermal Analysis. Before more accurately analyzing the thermal evolution of Yb:KGP crystals by powder XRD, we completed differential thermal analysis (DTA). We used a TA Instruments simultaneous differential techniques instrument SDT 2960. The analyses were made under an argon atmosphere using a gas flow of 90 cm^3/min and calcined alumina as reference material. Around 20 mg of powdered samples of $KYb_{0.029}Gd_{0.971}(PO_3)_4$ and $KYb_{0.045}Gd_{0.955}(PO_3)_4$ obtained from solution compositions of Yb_2O_3:Gd_2O_3:K_2O:P_2O_5 = x:6−x:34:60 mol %, with x = 0.3 and 0.6, respectively, were placed in a platinum pan and heated at 0.17 K/s from room temperature to 1273 K. The cooling process was not analyzed because of the irreversible transition of type III KLnP materials, with Ln = Gd and Nd.[16,17] To compare with the cyclic polymorph $KYb_xGd_{1-x}P_4O_{12}$[22] (type A; S.G. *C*2/c), about the same weight of a sample obtained from a solution with 1 at % ytterbium and composition Yb_2O_3:Gd_2O_3:K_2O:P_2O_5 = 0.06:5.94:34:60 was analyzed.

Yb:KGP Crystal Growth. The top-seeded solution growth−slow cooling (TSSG−SC) method without pulling was used to grow Yb:KGP single crystals. The equipment was the same as that used for the crystallization region studies. Around 200 g of solution, prepared the same as previously, had in this case an axial gradient around 1.2 K/mm. To begin the growth experiments, we used the same growth parameters as those previously optimized for KGP[17] and Nd-doped KGP[14] (see Table 1 for values and corresponding results). Crystals were grown therefore from the optimized solution composition of Yb_2O_3:Gd_2O_3:K_2O:P_2O_5 = x:6−x:34:60 mol % (experiments from 3 to 9) as long as the $P2_1$ phase crystallized. To grow crystals with an ytterbium concentration in solution either below 3 or above 10 at %, we had to use a solution composition of Yb_2O_3:Gd_2O_3:K_2O:P_2O_5 = x:4−x:36:60 mol % (experiments 1 and 10) to obtain the $P2_1$ crystalline phase. Crystals were grown on **a***-oriented paralepipedic seeds of Yb:KGP. This orientation ensures a suitable growth rate and avoids the possibility of losing the crystal because of the cleavage plane.[18] The rotation velocity of the seed was kept at 75 rpm because the viscosity of Yb-doped KGP solution was comparable to that of KGP or Nd-doped KGP solutions. Depending on the ytterbium concentration, we used a cooling rate of 0.1, 0.05, or 0.02 K/h. As in the case of Nd-doped KGP, the number of inclusions appearing in crystals increased when the ytterbium concentration also increased. Furthermore, polycrystallization occurred more frequently as the ytterbium concentration rose. The crystallization of various growth nuclei, probably due to the high viscosity of the solution, was also observed for the previously isostructurals but in this case it was much more usual. To avoid polycrystallization and succeed in growing inclusion-free single crystals, the cooling rate was decreased to 0.05 K/h from an ytterbium content in solution of 3 at %. From an ytterbium concentration in solution of 10 at %, even a slower cooling program, combining cooling rates of 0.02 and 0.05 K/h, was used (experiments 9−11). As previously, seeds were held on the same growth device equipped with a turbine, which is shown in reference 18.

Ytterbium Concentration Analysis. Electron probe microanalysis (EPMA) was used to determine the chemical composition of both crystals grown on a platinum disk and crystals grown by TSSG. The measurements were made using a CAMECA SX-50 operating at an accelerating voltage of 20 kV and an electron current of 100 nA. We used KYbW and KGP crystals grown by us as the standards for measuring Yb and K, Gd, P, and O, respectively. K and P were analyzed with the PET (Pentaery thritol, 002) crystal using the line Kα. O Kα was measured with a W/Si multilayer crystal and the Lα line of Yb and Gd were analyzed using the LIF (lithium fluoride, 200) crystal. The measurements were integrated for 10 s for all ions. From these results and the solution composition used in every case, the distribution coefficient of ytterbium in the structural sites of gadolinium were calculated using the expression $K_{Yb} = ([Yb]/([Yb]+[Gd]))_{crystal}/([Yb]/([Yb]+[Gd]))_{solution}$.

Raman Spectroscopy of Yb:KGP. The lattice vibrations of Yb:KGP and KGP were studied using the Raman technique. As the intermanifold electronic transitions of ytterbium are strongly coupled

(22) Ettis, H.; Naili, H.; Mhiri, T. *Cryst. Growth Des.* **2003**, *3* (4), 599.

Table 2. Crystalline Phase for Each Ytterbium Concentration and Solution Composition[a]

Yb at % in solution	molar ratio $(Yb_2O_3+Gd_2O_3)/K_2O$	phase	molar ratio $(Yb_2O_3+Gd_2O_3)/K_2O$	phase	molar ratio $(Yb_2O_3+Gd_2O_3)/K_2O$	phase
0.5	(0.075 + 14.925)/85	$P2_1 + C2/c$	(0.05 + 9.95)/90	$P2_1$	(0.025 + 4.975)/95	$P2_1$
1	(0.15 + 14.85)/85	$P2_1 + C2/c$	(0.1 + 9.9)/90	$P2_1$	(0.05 + 4.95)/95	$P2_1$
3	(0.45 + 14.55)/85	$P2_1$	(0.3 + 9.7)/90	$P2_1$	(0.15 + 4.85)/95	$P2_1$
5	(0.75 + 14.25)/85	$P2_1$	(0.5 + 9.5)/90	$P2_1$	(0.25 + 4.75)/95	$P2_1$
10	(1.5 + 13.5)/85	$P2_1$	(1.0 + 9.0)/90	$P2_1$	(0.5 + 4.50)/95	$P2_1$
15	(2.25 + 12.75)/85	$P2_1 + C2/c$	(1.5 + 8.5)/90	$P2_1$	(0.75 + 4.25)/95	$P2_1$
20	(3.0 + 12)/85	$P2_1 + C2/c$	(2.0 + 8.0)/90	$P2_1$	(1.0 + 4.0)/95	$P2_1$
30	(4.5 + 10.5)/85	$P2_1 + C2/c$	(3.0 + 7.0)/90	$P2_1$	(1.5 + 3.5)/95	$P2_1$
50	(7.5 + 7.5/85	$P2_1 + C2/c$	(5 + 5)/90	$P2_1$	(2.5 + 2.5)/95	$P2_1$

[a] The solution composition is expressed as a function of the $(Yb_2O_3+Gd_2O_3)/K_2O$ molar ratio with a constant P_2O_5 molar concentration of 60 mol %.

with lattice vibrations, the knowledge of the phonon frequencies can be useful in interpreting the substructure in absorption and emission spectra.

We cut and polished plate samples of about 1 mm thick KGP and $KYb_{0.029}Gd_{0.971}(PO_3)_4$ to do the measurements. The experimental setup comprised a Jobin-Yvon T64000 spectrophotometer with excitation by a CW argon laser (Coherent INNOVA 300, $\lambda =$ 514 nm). Behind the triple monochromator (1800 g/mm), the light was detected by a two-dimensional CCD matrix cooled with liquid nitrogen. A pre-monochromator eliminated the plasma discharge lines of the argon laser. A microscope (Olympus BH2) with high resolution was used to locate the laser spot in the sample. The laser power incident on the sample was about 60 mW. A backward scattering scheme was chose in order to increase the signal-to-noise ratio.

Optical Transmission of Yb:KGP. The optical transmission Yb:KGP was measured in the wavelength range from 0.175 to 10 μm. We used a Varian Cary 500 Scan spectrophotometer to do the measurements in the UV−visible and NIR regions up to 3.3 μm and an FTIR Midac Prospect spectrophotometer in the IR region. A 1 mm thick plate sample of $KYb_{0.029}Gd_{0.971}(PO_3)_4$ was cut and polished to do the measurements. The UV and IR cutoff values were calculated as the maximum transmission value divided by the *e* number. The ultraviolet region close to the UV cutoff is interesting from the point of view of the UV emitting sources pumping, such as Xe lamps. These highly energetic pumps cause often optical damage in the illuminated crystals. The susceptibility to optical damage, which is enhanced by the presence of dopants in the crystals, can shift the UV edge to longer wavelengths. As this shifting was clearer when measuring the absorption coefficient (α) rather than the transmission, we measured the optical absorption of $KYb_{0.029}Gd_{0.971}(PO_3)_4$, $KYb_{0.045}Gd_{0.955}(PO_3)_4$, and KGP between 175 and 500 nm.

Ytterbium Optical Absorption and Emission. We studied the optical absorption and emission of the ytterbium ion in the KGP host. A $KYb_{0.024}Gd_{0.976}(PO_3)_4$ crystal was cut and polished as an isometric 2 mm sided cube accurately oriented along the three principal optical axes N_p, N_m, and N_g. The optical absorption was measured in the 1 μm wavelength region using the same spectrophotometer as in the transmission measurements. The splitting of the Yb absorption band was also studied at 6 K equipping the spectrophotometer with a Leybold RDK-6-320 closed-cycle helium cryostat. The measurements were made by polarizing the incident beam parallel to each principal optical axis. The fluorescence spectra were recorded at both 300 and 10 K in 90° geometry with excitation by a 200 mW diode laser at 940 nm modulated at 1 kHz. The fluorescence was dispersed by a 0.46 m double monochromator (Jobin Yvon-Spex HR 460). We used a cooled Hamamatsu NIR R5509-72 photomultiplier for detection connected to a lock-in amplifier (EG&G, 7265 DSP). A close-cycle helium cryostat (Oxford CCC1104) was used to cool the sample for low-temperature measurements.

Results and Discussion

Crystallization Region of Yb:KGP. We determined how the type III Yb:KGP crystallization region evolved as a function of the ytterbium concentration close to the optimum composition zone previously determined. In this zone, the most optimum point to grow KGP single crystals was found to be Gd_2O_3:K_2O:P_2O_5 = 6:34:60 mol %. We have therefore kept the P_2O_5 concentration at 60 mol %. A higher P_2O_5 concentration leads to higher solution viscosity and consequently to lower growth rate and crystal quality. The crystallization region was also limited at a Gd_2O_3/K_2O molar ratio of 3/97 for the same reason. Above this ratio, the viscosity was too high for growing crystals, mostly because of the temperature, because as the Gd_2O_3/K_2O ratio decreased the saturation temperature also decreased. The boundaries of the crystallization region of Yb:KGP were defined by the intersection of the $(Yb_2O_3 + Gd_2O_3):K_2O$ isoconcentrational lines of 15:85, 10:90, and 5:95 with a P_2O_5 concentration of 60 mol % after studying several solution compositions. These isoconcentrational lines were, as for the other isostructural crystals, roughly coincident with the saturation temperature isotherms of 950, 880, and 825 K, respectively. Table 2 shows the crystalline phase identified for each ytterbium atomic percent and each tested solution molar ratio $(Yb_2O_3 + Gd_2O_3):K_2O$.

In the composition zone studied, Yb:KGP can crystallize into two different polymorphs, type III $KYb_xGd_{1-x}(PO_3)_4$ (S.G. $P2_1$) with long-chain geometry, and type A $KYb_xGd_{1-x}P_4O_{12}$ (S. G. $C2/c$) with cyclical geometry. Because of the centrosymmetrical structure of type A, second-order nonlinear optical processes are not allowed, so it cannot be used as a self-frequency doubling crystal. The high structural versatility of condensed polyphosphates has been extensively studied.[23,24] KGP crystallizes into these two polymorphs and even into a third one, type IV[25] (S. G. $P2_1/n$) also with long-chain geometry, which coincides with the structure of the ytterbium stoichiometric material, $KYb(PO_3)_4$ (KYbP).[26] Depending on the ytterbium concentration, the border between type III and type A varies. Although the ytterbium

(23) Palkina, K. K.; Chudinova, N. N.; Litvin, B. N.; Vinogradova, N. V. *Izv. Akad. Nauk, Neorg. Mater* **1981**, *17* (8), 1501.
(24) Durif, A. *Crystal Chemistry of Condensed Polyphosphates*; Plenum Press: New York, 1995.
(25) Rekik, W.; Naïli, H.; Mhiri, T. *Acta Crystallogr., Sect. C* **2004**, *60* (4), i−50.
(26) Palkina, K. K.; Maksimova, S. I.; Chudinova, N. N.; Vinogradova, N. V.; Chibisova, N. T. *Izv. Akad. Nauk, Neorg. Mater* **1981**, *17* (1), 110.

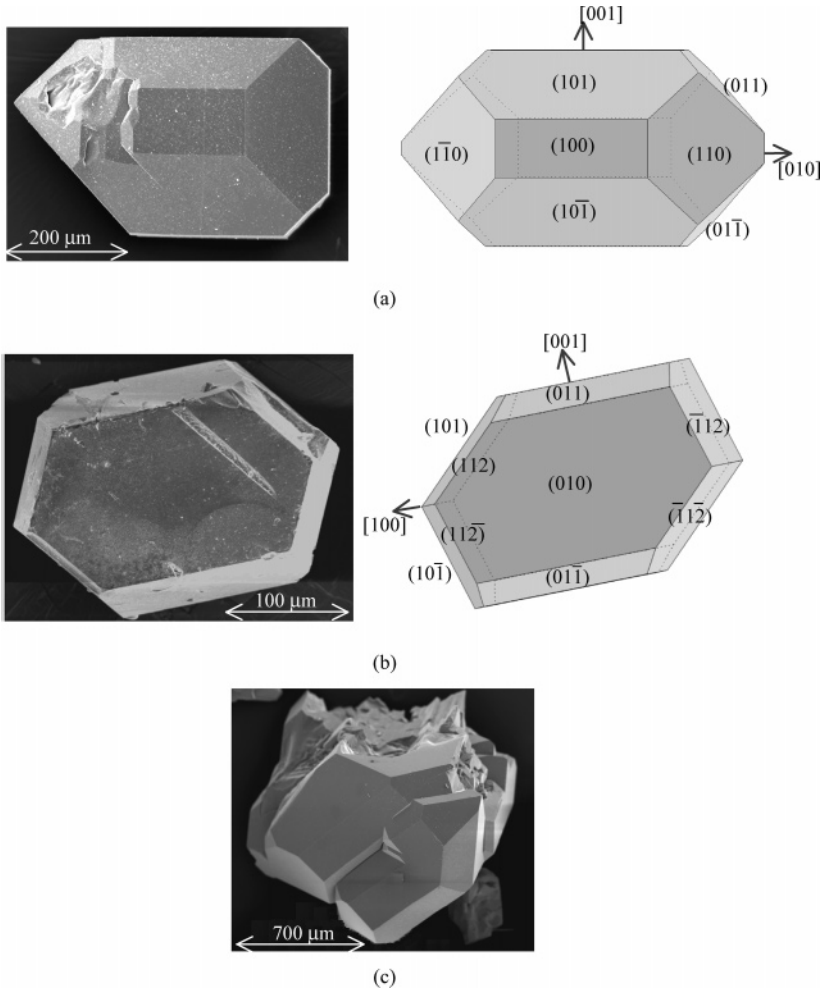

Figure 1. SEM photograph and morphological scheme of a small single crystal of (a) type III Yb:KGP (S.G. $P2_1$) with long-chain geometry and (b) type A Yb:$KGdP_4O_{12}$ (S.G. $C2/c$) with cycling geometry; (c) twinning on a Yb:KGP crystal.

concentration in solution was between 3 and 10 mol %, the $P2_1$ crystallization region border was placed above a (Yb_2O_3 + Gd_2O_3)/K_2O molar ratio of 15:85. This limit is similar to that of KGP, which is placed at a Gd_2O_3:K_2O molar ratio of 18:82 at 60 mol % P_2O_5. However, as the ytterbium concentration is either reduced or increased from this ytterbium concentration range, the border was shifted to a lower (Yb_2O_3 + Gd_2O_3):K_2O molar ratio and the $P2_1$ crystallization region was slightly narrowed (Table 2).

Figure 1 shows a SEM photograph and a morphological scheme drawn using the Software Shape utility[27] of both $P2_1$ and $C2/c$ phases. Any important morphologic change was observed when the ytterbium content in solution was increased but the light tendency to twinning (Figure 1c) was observed.

Yb:KGP Crystal Growth. We analyzed the Yb:KGP crystal growth process in order to manage to grow suitable sized inclusion-free single crystals. Among the different growth parameters that can affect the crystal quality, we analyzed the influence of the cooling rate. The composition of the growth solution was fixed by the stability of the $P2_1$ phase, taking into account the crystallization region previously determined. For any ytterbium concentration, the solution composition used was the most close to the optimum (Yb_2O_3 + Gd_2O_3):K_2O:P_2O_5 = 6:34:60 mol %. The high viscosity of this kind of solutions near the crystallization temperature around 923 K was μ = 16 Pa s for the same composition of a KGP solution[18] because of to the high polymerization degree of the phosphate compounds in the flux, mostly $Ln(PO_3)_3$, with Ln = Yb, Gd. The greater the viscosity, the slower the crystal growth process. The growth rate is therefore lower for a solution composition of (Yb_2O_3 + Gd_2O_3):K_2O:P_2O_5 = 4:36:60 mol % (experiments 1 and 10) and even lower for that of (Yb_2O_3 + Gd_2O_3):K_2O:P_2O_5 = 2:38:60 mol % (experiment 2). For a fixed solution composition, the saturation temperature slightly increases when the ytterbium content also increases. Polycrystallization also get out when the Yb_2O_3 content in solution increases, probably because of an increase in the solution viscosity. This higher tendency to polycrystallization may be related to the increase in twinning already observed on small crystals (Figure 1c) and never observed with KGP. Therefore, it was necessary to reduce the cooling rate in the first steps of the cooling program, when polynucleation can occur, for Yb_2O_3 concentrations from 10 at % in solution (experiments 9 and 10).

Ytterbium Doping in KGP. The chemical composition of crystals grown from solutions containing an 1, 3, 5, 10,

(27) Dowty, E. *Shape for Windows*, version 5.0.1.; Shape Software: Kingsport, TN, 1995.

Table 3. Ytterbium and Gadolinium Distribution Coefficients and Cell Parameters for Each Ytterbium Concentration (at %)

solution composition (mol %) Yb_2O_3:Gd_2O_3:K_2O:P_2O_5	Yb at % in solution	Yb at % in crystal	K_{Yb}	K_{Gd}	a (Å)	b (Å)	c (Å)	β (deg)	V (Å^3)
0.04:3.96:36:60	1	0.8	0.80	1.09	7.252(1)	8.352(1)	7.932(1)	91.67(1)	480.2(1)
0.18:5.82:34:60	3	1.8	0.61	1.01	7.250(1)	8.350(1)	7.930(1)	92.68(1)	479.9(1)
0.3:5.7:34:60	5	2.9	0.57	1.03	7.249(1)	8.347(1)	7.928(1)	91.69(1)	479.5(1)
0.6:5.4:34:60	10	4.5	0.45	1.07	7.247(1)	8.343(1)	7.921(1)	91.71(1)	478.7(1)
0.6:3.4:36:60	15	6.6	0.44	1.02	7.245(1)	8.339(1)	7.916(1)	92.74(1)	478.0(1)
0.8:3.2:36:60	20	11.6	0.58	1.10	7.242(1)	8.334(1)	7.904(1)	92.78(1)	476.8(1)
1.2:2.8:36:60	30	19.9	0.66	1.14	7.237(1)	8.324(1)	7.892(1)	92.82(1)	475.2(1)
2:2:36:60	50	29.8	0.60	1.40	7.231(1)	8.310(1)	7.873(1)	92.90(1)	473.1(1)

15, 20, 30 and 50 at % ytterbium was determined by EPMA. Table 3 shows the ytterbium distribution coefficients in the structure, defined as $K_{Yb} = ([Yb]/([Yb]+[Gd]))_{crystal}/([Yb]/([Yb]+[Gd]))_{solution}$ and the ytterbium atomic percent in solution and in crystal. As the ionic radius of ytterbium is only around 6.5% smaller than that of gadolinium, an ytterbium distribution coefficient close to the unit was expected. However, not only was it lower for all the ytterbium concentrations but it also decreased as the ytterbium content increased until it stabilized around half the unit. The crystal cell parameters *a*, *b*, *c*, and *V* slightly decreased as the concentration of ytterbium increased in crystals because it progressively substituted gadolinium in its structural position. All cell parameters evolved linearly with the concentration. Figure 2 shows the average change in each cell parameter ($\Delta Y/Y$) versus the concentration. In Table 3 are listed the cell parameter values for each ytterbium concentration.

Thermal Stability and Phase Transitions. We analyzed how Yb:KGP evolved with temperature between 298 and 1273 K. By differential thermal analysis (DTA), we determined that both $KGd_{0.029}Gd_{0.971}(PO_3)_4$ and $KGd_{0.045}Gd_{0.955}(PO_3)_4$ decomposed at 1130 K (Figure 3). The transition temperature was lower than that of KGP, which shows an endothermic peak at 1142 K. The polymorph $KGdP_4O_{12}$ *C*2/*c* (type A) decomposed at a slightly higher temperature (1138 K). These results agreed with those of the isostructurals $KSm(PO_3)_4$ and $KSmP_4O_{12}$,[28] which decompose at 1133 and 1145 K, respectively. The weight change during the experiments was rather imperceptible.

The decomposition of $KGd_{0.029}Gd_{0.971}(PO_3)_4$ was more accurately studied by X-ray powder diffraction. Figure 4 shows the X-ray pattern at room temperature and the selected patterns at several temperatures that describe the thermal evolution in both the heating and the cooling processes. The crystal phases evolved in the phase transition were identified as $GdPO_4$ (83-0657 ICDD database[29]), orthorhombic $Gd(PO_3)_3$ (isostructural to $Eu(PO_3)_3$ 31-0519 ICDD database[30]), $Gd_2P_4O_{13}$ (35-0078 ICDD database[31]), and GdP_5O_{14} (73-1068 ICDD database[32]). All these crystal phases were also present during the decomposition of KGP[17] except GdP_5O_{14}, which was, however, identified as the neighboring phase in the richest P_2O_5 zone of the KGP crystallization region. This phase (GdP_5O_{14}) appeared at 1223 K in the heating process and disappeared at 1173 K in the cooling process. $Gd(PO_3)_3$ appeared as the only phase at 1173 K but the intensity of its peaks quickly reduced between this temperature and 1273 K, when it completely disappeared. As the intensity of the peaks of $Gd(PO_3)_3$ decreased, that corresponding to the rest

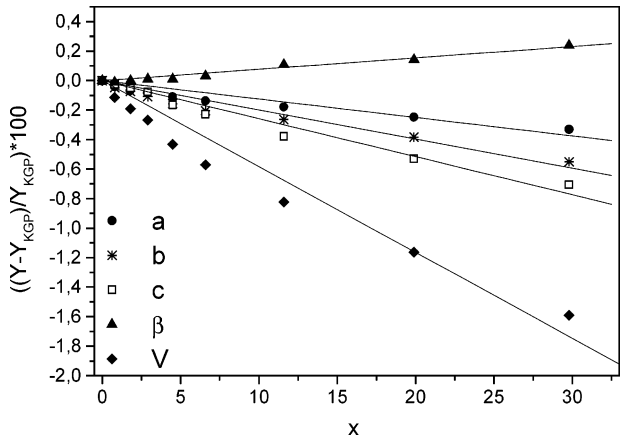

Figure 2. Relative evolution of the cell parameters and unit-cell volume of $Yb_xGd_{1-x}(PO_3)_4$ as a function of the ytterbium content in KGP.

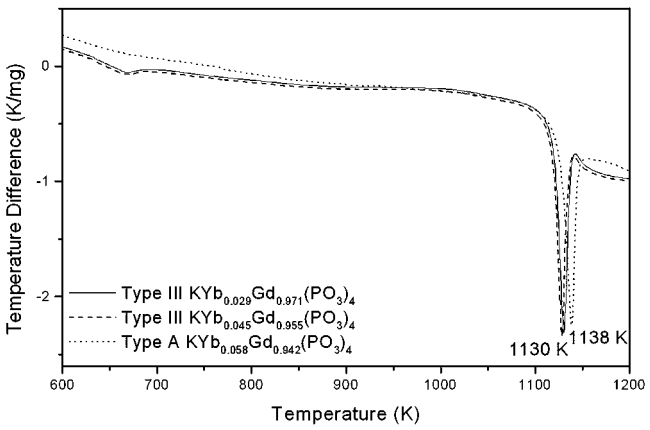

Figure 3. Differential thermal analysis thermogram of type III $KYb_{0.029}Gd_{0.971}(PO_3)_4$ crystal, type III $KYb_{0.045}Gd_{0.955}(PO_3)_4$ crystal, type A $KYb_{0.006}Gd_{0.994}P_4O_{12}$ crystal.

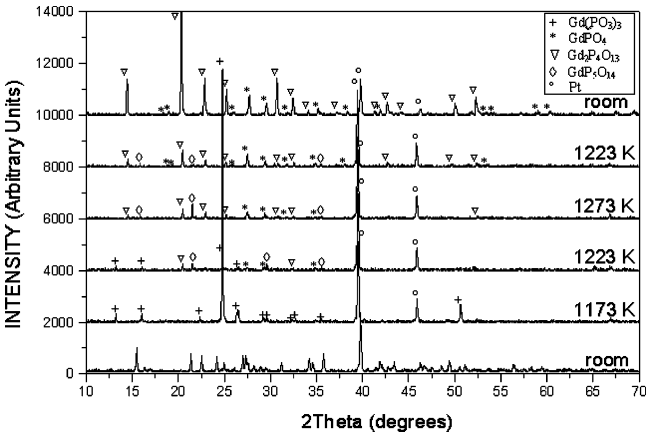

Figure 4. X-ray powder diffraction pattern at room temperature of $KYb_{0.029}Gd_{0.971}(PO_3)_4$ and selected patterns at several temperatures describing its evolution with temperature in both heating and cooling processes.

of the phases steadily increased in the same temperature range. $GdPO_4$ and $Gd_2P_4O_{13}$ remained and even slightly increased its intensity from this temperature until room temperature. Because of the dilation of the material, a slight displacement of the peaks was observed in the last pattern at room temperature. The most important difference in the thermal evolution caused by the presence of the ytterbium ion was that $Gd_2P_4O_{13}$ remained until room temperature but completely transformed into $GdPO_4$ for undoped KGP. The final product of the Yb:KGP thermal decomposition was therefore a mixing of both phases.

From powder XRD analysis and DTA, we determined that Yb:KGP decomposed at 1130 K into $Gd(PO_3)_3$. However, between this temperature and 1273 K it completely transformed into $GdPO_4$, $Gd_2P_4O_{13}$, and GdP_5O_{14}. This last phase completely disappeared at 1173 K in the cooling process. An amorphous phase composed by potassium and phosphorus oxides was also present because the sample weight remained roughly constant. The endothermic peak observed in the thermogram at 1130 K may be related to this decomposition.

Yb:KGP slightly dilated as the temperature increased. This thermal expansion was comparable to that of KGP [17] and also was almost isotropic.

Raman Spectroscopy. Raman spectroscopic properties of phosphate crystals and glasses have been extensively studied. Mostly, the Raman spectra have been related to the vibrational motions of simple structural units, but in the random network approach, it is necessary to consider the local geometry of the phosphate units. Metaphosphates with a [O]:[P] ratio of 3 have a geometry of chains or cycles.[33] However, the Raman spectra are qualitatively the same. The spectra are neither affected by the number of repetitive units $(PO_3)_x$ that generate the chains or cycles or by the lanthanide or alkali ions in the structure. The spectra therefore have the same characteristic peaks for metaphosphates of lanthanide $Ln^{III}(PO_3)_3$, with Ln = Gd[34] Sm,[35] La,[36] or poyphosphates $M^{I}Ln^{III}(PO_3)_4$, such as $KBi(PO_3)_4$[37] or $M^{I}La(PO_3)_4$ with M^{I} = Na, Ag,[38] which have a chain geometry and $P2_1/n$ as space group, and $KSm(PO_3)_4$,[39,40] which is isostructural to KGP. All these Raman spectra have two characteristic strong peaks around 1185 and 700 cm^{-1}. The strong peak around 1185 cm^{-1}, which is accompanied by some other weaker peaks in the region from 1000 to 1300 cm^{-1}, is a common feature to materials built from linked PO_4 tetrahedra. This peak is generally attributed to the symmetric stretching vibration ν_s of the PO_2 group corresponding to the motion of the nonbridging oxygen. The weaker peaks around it are assigned to symmetric ν_s and antisymmetric ν_a vibrations of the same group. The strong peak around 700 cm^{-1} is attributed to the symmetric stretching vibration ν_s of the P−O−P chain linkage. Very weak peaks attributed to symmetric ν_s and antisymmetric ν_a vibrations of the same group are often observed in the region from 650 to 1000 cm^{-1}. Peaks around this region are a useful indicator of the structure of metaphosphate. Figure 5 shows the Raman spectra of Yb:KGP and KGP. All metaphosphate characteristic peaks above-described are present. In the region of 700 cm^{-1}, two strong peaks at 728 and 671 cm^{-1} are observed that are due to the different positions of the lanthanide and alkali ions giving different frequencies of the P−O−P ν_s.[40] In the low-frequency region below 650 cm^{-1}, it is very difficult to distinguish the symmetric and antisymmetric bending modes of PO_2 and P−O−P groups.

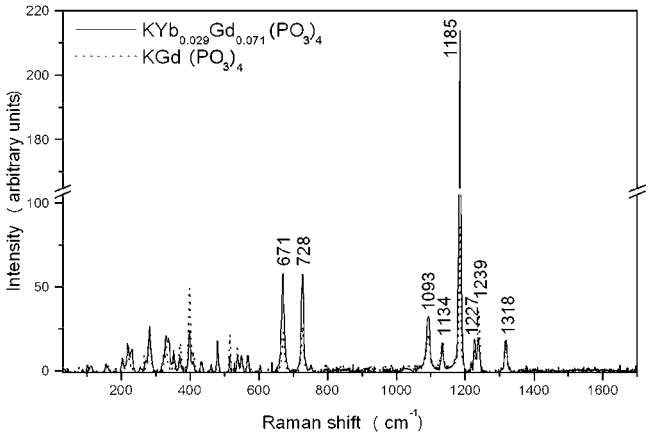

Figure 5. Raman spectra of $KYb_{0.029}Gd_{0.971}(PO_3)_4$ and $KGd(PO_3)_4$ at room temperature.

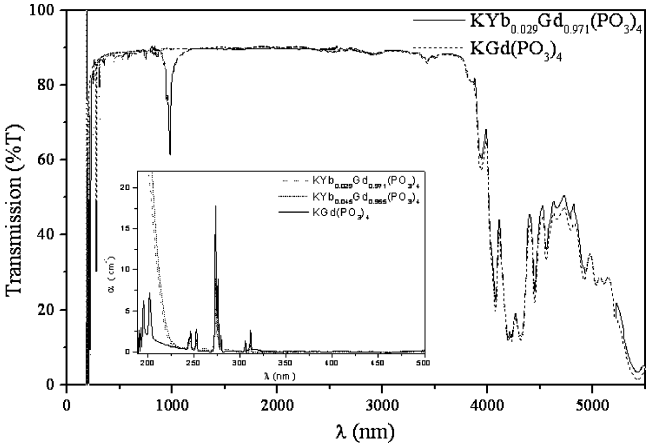

Figure 6. (a) Transparency window of $KYb_{0.029}Gd_{0.971}(PO_3)_4$ at room temperature. Inset: evolution of the UV cutoff wavelength with the concentration of ytterbium.

Optical Transmission. Figure 6 shows the transparency window of $KYb_{0.029}Gd_{0.971}(PO_3)_4$. The IR cutoff wavelength is around 5.5 μm because of the absorption resonance of

(28) Ferid, M.; Ariguib, N. K.; Trabelsi, M. *J. Solid State Chem.* **1987**, *69* (1), 1.
(29) Mullica, D. F.; Grossie, D. A.; Boatner, L. A. *Inorg. Chim. Acta* **1985**, *109* (2), 105.
(30) Tsujimoto, Y. *J. Electrochem. Soc.* **1977**, *124*, 533.
(31) Agrawal, D.; Hummel, J. *J. Electrochem. Soc.* **1980**, *127*, 1550.
(32) Bagieu-Beucher, M.; Duc, T. Q. *Bull. Soc. Fr. Mineral Crystallogr.* **1970**, *93*, 505.
(33) Hong, H. Y. G. *Mater. Res. Bull.* **1975**, *10* (7), 635.
(34) Ileva, D.; Jivov, B.; Kovacheva, D.; Tsacheva, Ts.; Dimitriev, Y.; Bogachev, G.; Petkov, Ch. *J. Non-Cryst. Solids* **2001**, *293*−*295*, 562.
(35) Mierzejewski, A.; Saunders, G. A.; Sidec, H. A. A. *J. Non-Cryst. Solids* **1988**, *104* (2−3), 323.
(36) Hall, D. W.; Brawer, S. A., Weber, M. J. *Phys. Rev.* **1982**, *25* (4), 2828.
(37) Jaouadi, K.; Naïli, H.; Zouari, N.; Mhiri, T. Daoud, A. *J. Alloys Compd.* **2003**, *354* (1−2), 104.
(38) El Masloumi, M.; Imaz, I.; Chaminade, J.-P.; Videau, J.-J.; Couzi, M.; Mesnaoui, M.; Maazaz, M. J. *J. Solid State Chem.* **2005**, *178* (11), 3581.
(39) Mokhtar, F., Ariguib, N. K. Trabelsi, M. *J. Solid State Chem.* **1987**, *69* (1), 1.
(40) Saito, M.; Honma, T.; Benino, Y.; Fujiwara, T; Komatsu, T. *Solid State Sci.* **2004**, *6* (9), 1013.

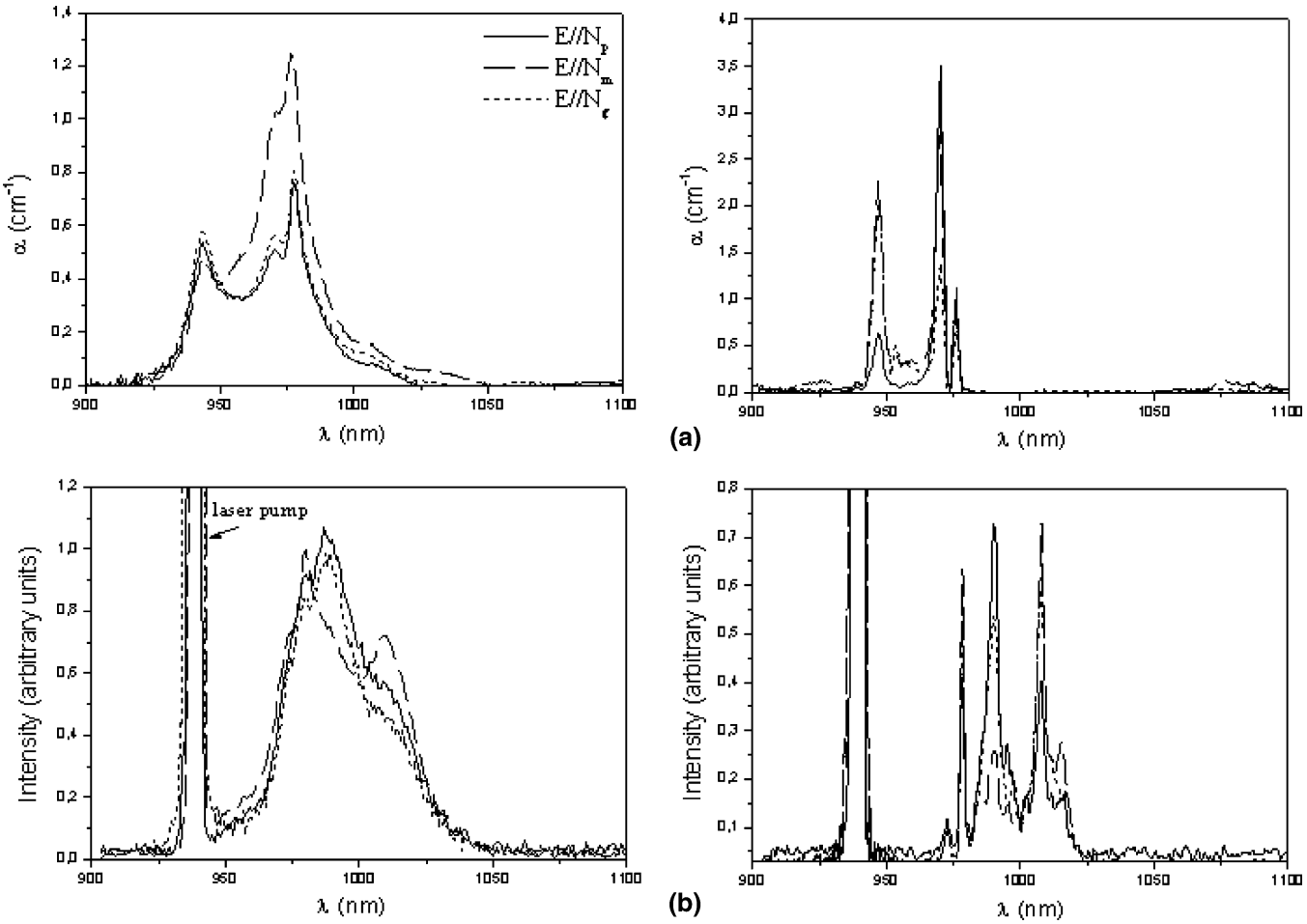

Figure 7. (a) Polarized optical absorption spectra of $KYb_{0.024}Gd_{0.976}(PO_3)_4$ at room temperature and 6 K. (b) Polarized emission spectra of $KYb_{0.024}Gd_{0.976}(PO_3)_4$ at room temperature and 10 K.

the P−O linkage as in the case of KGP. From this wavelength, the transparency window extends to approximately 200 nm. The UV cutoff wavelength in this region shifted to longer wavelengths with the increase of the ytterbium content in the KGP host, e.g., at 205 nm for $KYb_{0.029}Gd_{0.971}(PO_3)_4$ and 208 nm for $KYb_{0.045}Gd_{0.955}(PO_3)_4$ (inset in Figure 6), probably due to the higher susceptibility of doped crystals to optical damage. The strong absorption band close to 1 μm is attributed to the ytterbium transition $^2F_{7/2} \rightarrow {}^2F_{5/2}$.

Ytterbium Optical Absorption and Emission. The polarized optical absorption and emission spectra of Yb^{3+} in KGP at room temperature and 6 K are shown in Figure 7. The ytterbium concentration of the $KYb_{0.024}Gd_{0.976}(PO_3)_4$ cube used for measurements was 1.007×10^{20} cm^{-3}.

The absorption band associated with the ytterbium transition $^2F_{7/2} \rightarrow {}^2F_{5/2}$ in KGP extends from 1025 to 925 nm at room temperature and is characterized by three main peaks centered at 945, 970, and 978 nm. As ytterbium has an odd number of electrons in the 4f shell, polarization-dependent selection rules are not expected but intensity variation of the peaks is still possible. The dichroism for Yb:KGP is quite low, but the absorption intensity is higher for $E:N_m$.

The peaks in the fluorescence spectra correspond to the emission from the excited state $^2F_{5/2}$ manifold to the four sublevels of the ground state manifold $^2F_{7/2}$. From the low-temperature polarized fluorescence spectra, we determined the four sublevels of the ground state $^2F_{7/2}$. Four main lines were found at 976, 988, 1005, and 1014 nm accompanied with phonon added peaks. These correspond to the transitions $^2F_{5/2}(0') \rightarrow {}^2F_{7/2}(0)$, $^2F_{5/2}(0') \rightarrow {}^2F_{7/2}(1)$, $^2F_{5/2}(0') \rightarrow {}^2F_{7/2}(2)$, and $^2F_{5/2}(0') \rightarrow {}^2F_{7/2}(3)$, respectively.[19]

Conclusions

We successfully grew ytterbium-doped KGP single crystals by TSSG-SC in spite of the high solution viscosity, around 16 Pa s, and the usual polycrystallization. Crystals can be grown using the same solution composition previously optimized for undoped or Nd-doped KGP as long as the ytterbium concentration is between 3 and 10 at % in solution. The concentration of ytterbium in solution is either lower than 3 at % or higher than 10 at % and up to 50 at %; the $P2_1$ crystallization region is slightly narrowed and moved toward a lower $(Yb_2O_3+Gd_2O_3):K_2O$ molar ratio since it is the neighboring phase $C2/c$ which crystallizes. Polymorphism of Yb:KGP between the long-chain and cyclical structures is not strange because it is a well-known feature of this type of condensed polyphosphates. The rotation velocity and seed orientation are the same as those used to grow Nd-doped KGP. However, the cooling rate has to be decreased to 0.02 K/h in the first steps of the growth process to obtain Yb:KGP crystals free of macroscopic defects because of polycrystallization. Up to now, we have successfully grown inclusion-free single crystals with a maximum ytterbium

concentration in solution of 15 at %, hence around 7.5 at % in crystal because the actual ytterbium concentration in the crystal was found to be reduced to about half of that in solution. Nevertheless, we found that the $P2_1$ phase of Yb:KGP can crystallize from solutions with an ytterbium concentration up to 50 at %. So, taking into account that the ytterbium concentration in crystal would be reduced by about half, an ytterbium doping level around 25−30 at % may be reached in single crystals grown by TSSG-SC. The self-frequency doubling properties will therefore not be limited by the active ion concentration unlike other well-known nonlinear crystals. Too high ytterbium doping levels can reduce the laser efficiency due to reabsorption, so further spectroscopic and laser investigations are necessary to determine the optimum ytterbium doping level. A slight decrease in the cell parameters with the introduction of ytterbium in the KGP structure has been determined for any ytterbium concentration from 1 to 50 at % in solution. The actual concentration in crystals has been also determined for each of them. Yb:KGP decomposes irreversibly at 1130 K and after crystalline transformations, which occurred between this temperature and 1173 K during cooling;, two final products remained at room temperature, $GdPO_4$ and $Gd_2P_4O_{13}$. The ytterbium ions in KGP cause the slight shifting of the UV cutoff to longer wavelengths, though it continues to be quite low. Yb:KGP and KGP show the typical vibrational structure of metaphosphates. The optical absorption and emission of ytterbium in the KGP host have been measured.

Acknowledgment. The authors acknowledge financial support from Fons Social Europeu i del Departament d'Universitats, Recerca i Societat de la Informació de la Generalitat de Catalunya under Project 2005SGR658 and personal support 2006FIC00469, and MEC (Ministerio de Educación y Ciencia of the Spanish government) of the Spanish government) under Projects MAT-05-06354-C03-02, MAT-04-20471-E, and CIT-020400-2005-14.

CM0621242